*Int. J. Heat Mass Transfer.* Vol. 34, No. 1, pp. 267–280, 1991
Printed in Great Britain

0017–9310/91 $3.00+0.00


# Evaporation from a packed bed of porous particles into superheated vapor

JAMIL A. KHAN,† DONALD E. BEASLEY and BULENT ALATAS
Thermal-Fluid Sciences Research Laboratory, Department of Mechanical Engineering, Clemson University, Clemson, SC 29634-0921, U.S.A.

(*Received* 1 *May* 1989 *and in final form* 13 *March* 1990)

**Abstract**—An experimental and computational study of evaporation into superheated steam from porous particles, which form a packed bed, is performed. The goal of the study is to develop a predictive model of the drying process in packed beds with steam as the drying medium. The direct experimental measurement using load cells of the weight of alumina particles of various diameters in a packed bed during the drying process produced a complete continuous drying curve. A range of experimental conditions are examined, and a correlating equation for the overall heat transfer coefficient developed. Evaporation from a single spherical porous particle is modeled as occurring at a receding liquid/vapor interface within the particle. The drying process in a single particle is assumed to be thermally controlled. The single particle model is incorporated into an overall model for drying in a packed bed. The model predicted overall and local drying rates, as well as transient temperature distributions in the packing. The results of this study indicate that drying in a packed bed of significant depth occurs in three phases. The three phases of drying correspond to periods where the entire bed is in the constant drying rate regime, portions of the bed have entered the falling rate regime, and the entire bed is in the falling rate regime, respectively. The existence of these phases of drying are confirmed by both measured temperature distributions and measured drying rates. Predictions of the overall drying rate from the model show favorable agreement with measured drying curves.

## INTRODUCTION

DRYING is one of the most important, energy intensive industrial processes. The drying process consumes much of the energy used in several industries, including textiles and pulp and paper and the food industry. Some form of dehydration is carried out in almost all chemical processing industries. It is clear that the development of more effective drying processes will provide for energy conservation, and in some cases will have significant economic impact. Superheated steam drying of solids presents numerous distinct advantages over conventional air drying, especially for products which are not temperature sensitive. There are two basic approaches to the use of steam as a drying medium. In the direct drying process, steam contacts the material being dried. Generally this material is porous and in granular form or in thin layers, such as paper or textiles. Indirect drying involves the transfer of energy through an intervening surface; possible geometries include tube bundles or steam jackets. The thermal conductivity of porous materials greatly decreases with decreasing moisture content, and thus indirect drying is not effective in achieving a high degree of dryness. A candidate approach to steam drying involves multiple effect dryers, where both direct and indirect drying is used to provide efficient energy utilization. For such a drying process, the steam exiting the initial stage of drying could be recompressed, and if necessary reheated, and subsequently recycled to another stage of the drying process. Significant energy savings may thus be realized, as discussed by Potter [1]. Currently operating plants world-wide have experienced significant energy savings, over conventional air drying, using steam as the drying medium.

The present study is directed towards the characterization of the drying of moist porous granular solids in a packed bed dryer, using steam as the working fluid. Previous studies of air drying in packed beds concentrated mainly on the determination of an expression for the convective heat transfer coefficient, or the overall drying rate. The objectives of the present study include the development of a model for packed bed drying in superheated steam, and the experimental investigation of the drying rate and heat transfer in a superheated steam packed bed dryer. It is desired to model the drying process under conditions where the drying rate is thermally controlled, or in other words the rate of evaporation from an individual particle is determined solely by the convective heat transfer at the surface and conduction through the particle to a receding liquid/vapor interface. The experimental study provides the continuous measurement of the total weight of the packed bed, with simultaneous measurement of the temperature distribution in the bed. As far as is known, no previous study has directly

† Present address: Department of Mechanical Engineering, University of South Carolina, Columbia, SC 29208, U.S.A.

## NOMENCLATURE

| | |
|---|---|
| $a$ | surface area per unit volume in packed bed |
| $c$ | specific heat capacity |
| $c_0$ | reference specific heat |
| $Bi$ | Biot number |
| $Bi_1$ | Biot number, $hR'/k_1$ |
| $Bi_2$ | Biot number, $hR'/k_2$ |
| $h$ | heat transfer coefficient |
| $h_{fg}$ | latent heat of vaporization |
| $k$ | thermal conductivity |
| $k_e^\lambda$ | axial effective thermal conductivity |
| $k_0$ | reference thermal conductivity |
| $N$ | number of grid locations; the $N$th grid location is at the surface of the sphere |
| $p$ | distance of interface location from nearest grid location in the direction of surface of the sphere |
| $r$ | radial coordinate, $r'/R'$ [dimensionless] |
| $r'$ | radial coordinate [dimensional] |
| $r_0$ | radial location of the drying interface, $r'_0/R'$ [dimensionless] |
| $r'_0$ | dimensional radial location of the drying interface |
| $\Delta r$ | radial spatial increment |
| $R'$ | sphere radius |
| $t'$ | time [dimensional] |
| $t$ | dimensionless time |
| $\Delta t$ | time step |
| $T$ | solid temperature [dimensionless] |
| $T'$ | dimensional solid temperature |
| $T_i^j$ | temperature (dimensionless) at the $i$th radial node and the $j$th time step |
| $T'_\infty$ | free stream temperature |
| $T_\infty$ | dimensionless free stream temperature, see equation (3) |
| $T_{si}^j$ | dimensionless surface temperature of the particle at the $i$th grid point and the $j$th time step |
| $u$ | axial fluid velocity in packed bed |
| $x$ | axial coordinate |
| $\Delta x$ | axial spatial increment. |

Greek symbols

| | |
|---|---|
| $\beta$ | defined parameter (see equation (2)) |
| $\varepsilon$ | void fraction within the packed bed |
| $\rho$ | density |
| $\rho_l$ | liquid density |
| $\rho_0$ | reference density |
| $\phi$ | void fraction within an individual particle |
| $\chi$ | fluid temperature |
| $\psi$ | ratio of moisture content to initial moisture content. |

Subscripts

| | |
|---|---|
| 1 | wet region |
| 2 | dry region |
| $\infty$ | free stream convective environment |
| 0 | reference (saturated steam at 23.89°C) |
| in | initial |
| sat | saturation. |

and continuously measured the drying of a packed bed of porous particles in a steam environment. The flow rate of steam to the bed, the size of the particles, and the degree of superheat were studied over an appropriate range. The model predictions for drying rate were compared with measured data.

## BACKGROUND

The drying of moist porous solids involves numerous complex processes; accordingly, drying behavior can be influenced by a large number of independent variables, including such factors as solid density, permeability, and hygroscopicity. Although drying processes have historically been very common, and generally consume significant quantities of energy, fundamental research into the drying process was not carried out until the beginning of this century. The first engineering analysis of drying was performed by Lewis [2], who postulated that drying occurred in two processes: diffusion of moisture to the surface from the interior of the solid, and subsequent evaporation of the moisture from the surface of the solid. Sherwood [3] and Gilliland and Sherwood [4] applied the diffusion theory to the drying of solids. At about the same time, the soil science community realized the importance of capillarity in the migration of moisture, and thus in the drying process [5, 6]. In describing drying in terms of diffusion or capillary theories, the role of heat transfer in the drying process was neglected. Krischer [7] explicitly considered the importance of energy transport in the drying process. Phillip and De Vries [8] extended the previous treatments of drying to include the effects of capillary flow and vapor transport, and incorporated the thermal energy equation into the set of governing equations that describe the drying process. Empirical input was necessary for closure of the model.

More recently, numerous studies have addressed the drying problem. A mathematical model of drying in a rectangular two-dimensional geometry was developed by Berger and Pei [9]. In this geometry, the top surface was exposed to a convective environment, and the other three faces were insulated; a computational solution was accomplished. Luikov [10] developed a model of the drying process by assuming that the transfer of moisture is analogous to heat transfer, and that capillary transport is proportional

to gradients in moisture and temperature. The resulting transport coefficients require extensive experimental determination. Stanish *et al.* [11] addressed the problem of drying of hygroscopic media; the objective of this work was to develop a reliable, realistic model of the phenomenon. Their proposed model includes the combination of all pertinent transport mechanisms into a single generalized model. Min and Emmons [12] and Dayan and Gluekler [13] have modelled drying in terms of evaporation from a receding interface in a semi-infinite strip, under intense drying conditions.

The concept of superheated steam drying was examined in a limited way by Hausbrand [14]. Wenzel and White [15] provided a quantitative basis for comparing air and steam as drying media for granular materials. In this early examination of steam drying, it was concluded that steam does not alter the general characteristics of drying, and that the drying rate was limited only by the heat transfer coefficient. Yoshida and Hyodo [16] and Hasan *et al.* [17] investigated steam drying in terms of an inversion temperature. The inversion temperature is the temperature above which steam drying is faster than air drying.

The mathematical description of drying in a superheated steam environment has received some recent attention. Loo and Mujumdar [18] developed a simulation model for combined impingement and through drying of paper, using steam as the drying medium. Meunier and Munz [19] developed a one-dimensional model of a flash dryer operating in the constant drying rate period. Salin [20] provided quantitative analysis of wood drying in superheated steam. None of these analyses have addressed steam drying in a packed bed geometry.

Kato *et al.* [21] investigated a packed bed dryer using air as the drying medium; a model of the drying rate in a packed bed was developed, and combined with heat transfer data to predict the drying of activated alumina. The effects of superficial gas velocity, bed height, particle diameter, and inlet gas temperature on the drying characteristics were investigated. Hasatani and Arai [22] derived the basic differential equations controlling the temperature and concentration fields in a packed bed of fine particles, and solved the equations for a general case of unsteady heat and mass transfer to air.

Two recent studies have modeled drying as occurring at a receding interface between wet and dry regions in a spherical geometry. Agarwal *et al.* [23] modeled the drying and devolatization of a spherical coal particle in a fluidized bed. This study models the evaporation process as occurring at a receding front within the coal particle; the temperature distribution in the dry region is determined from an approximate temperature profile in the particle and a pseudo-steady model of the surface temperature. Cheong *et al.* [24] modeled the drying of slurry droplets where the drying slurry formed a crust of solid material. In this model, the interface temperature is not prescribed; a linear temperature profile was assumed within the solid crust, while the central region is modeled as a lumped thermal capacitance system.

## EXPERIMENTAL INVESTIGATION

The experimental apparatus was designed to provide a controlled, measured flow rate of superheated steam, at a known thermodynamic state, to the packed bed test section. A schematic drawing of the experimental apparatus is shown in Fig. 1. Steam was supplied from the university physical plant at a pressure of 830 kPa, and a quality of 90–95%. The supply steam was expanded in a pressure regulator to the working pressure of 130–210 kPa. The steam then passed through an ERDCO series 400 steam flow meter used to monitor the flow rate for control purposes, and through a flow regulating valve. The regulated steam then passed through two circulation type steam superheaters, each with a capacity of 9 kW. A temperature controller ensured that the steam temperature remained within 0.6°C of the set point during an experimental run. Upon leaving the superheaters, the steam entered the test section or flowed through a by-passs during the start-up of the apparatus. By-passing of the steam and preheating of the housing using guard heaters allowed essentially a step-change inlet condition to the test bed to be achieved. The steam flow rate was observed to be steady within 2% during any experimental run. The guard heaters essentially eliminated radial heat transfer within the test bed; energy losses without guard heating were less than 4% of the superheat energy content of the steam, and essentially negligible with controlled guard heating.

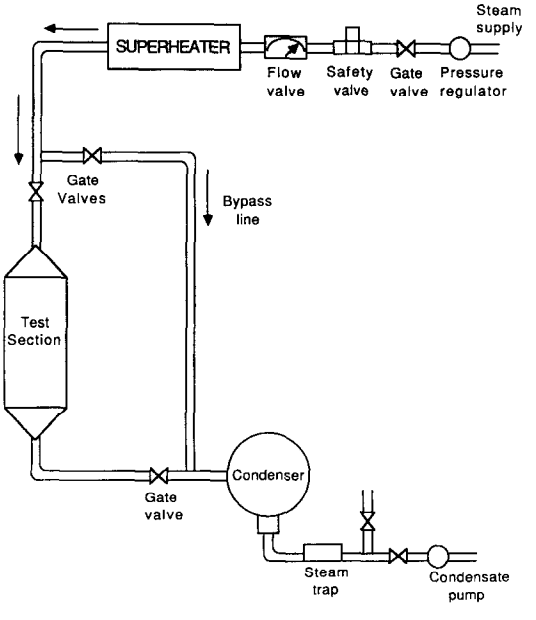


FIG. 1. Schematic of the experimental facility.

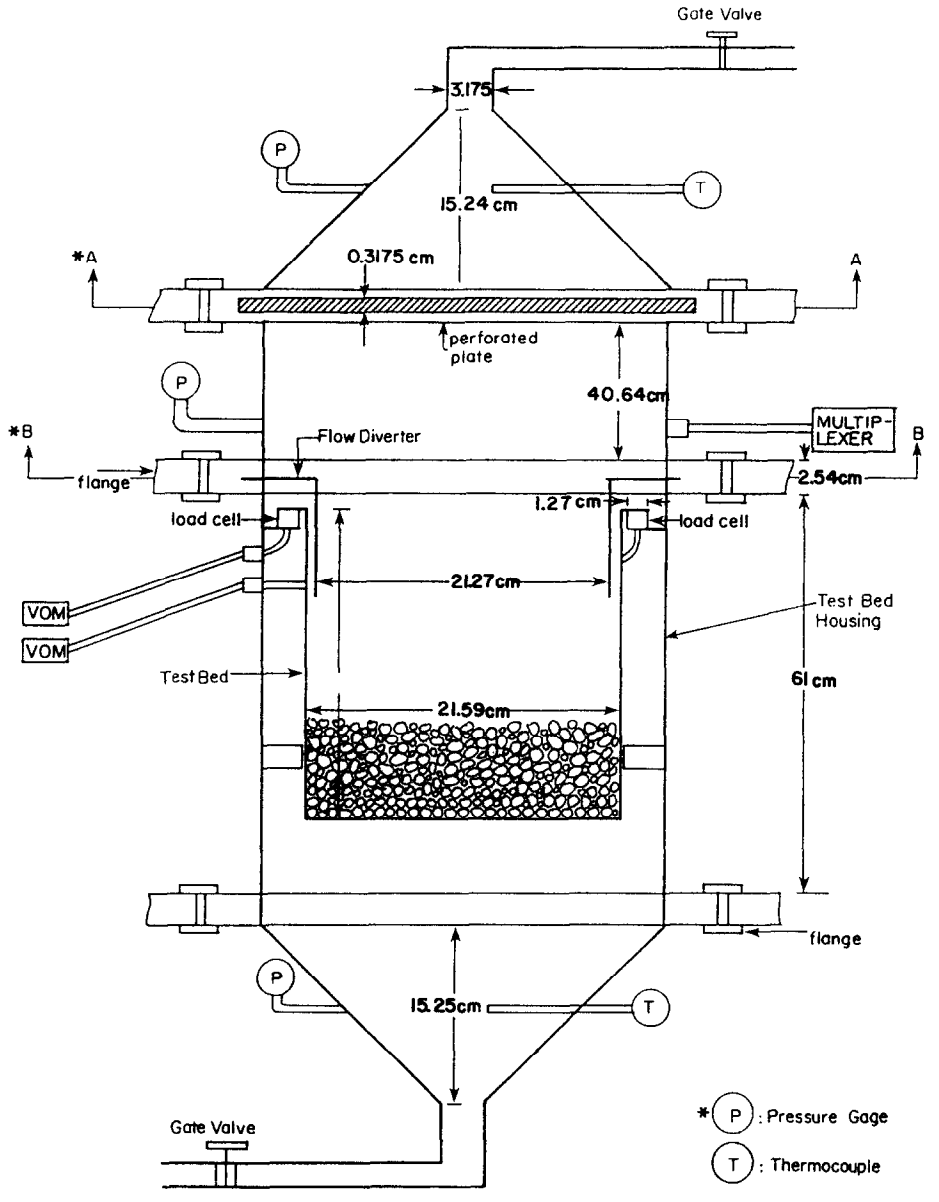


FIG. 2. Details of the test section design.

In order to provide a uniformly distributed flow of steam across the cross section at the inlet to the packed bed, a porous sintered stainless steel plate having 20 $\mu$m pores was mounted at the flanged connection of the test section, upstream of the bed. The test section was composed of a housing made of stainless steel pipe (25.4 cm diameter), and a test bed. The cylindrical test bed was made of 18 gage aluminum sheet, with the particles supported at the bottom by a perforated plate. As shown in Fig. 2, the test bed was isolated from the stainless steel housing, and supported by a protruding flange at the top. This flange rested on two compression type miniature load cells [ELF-500W-20(HW/12)], manufactured by Entran Devices, Inc., Fairfield, New Jersey. The load cells were custom designed to withstand a steam environment of 300°C. The load cells were placed on two seats welded to the test section housing, as shown in the figure. To prevent steam from flowing between the test bed and the housing, a flow diverter was installed at section B–B, and appropriately sealed to the test bed in such a way as to not influence the load cell output.

The parameters measured during an experimental run were the mass flow rate of steam, the weight of the test bed, as measured by the load cells, the inlet steam conditions, and the temperature distribution within the packing of particles. The temperature compensated load cells provided a continuous record of

the weight of the packing particles. Output from the load cells was monitored by Keithley Model 179A multimeters, with 0.01 mV resolution. The load cells were calibrated prior to installation, and the calibration periodically confirmed. The temperature of the particles were measured using eleven 40-gage J-type thermocouples, with eight placed axially along the centerline of the packed bed, and three at various other radial locations. Three thermocouples were placed inside the particles and five in the steam environment touching the surface of the particles; the thermocouple wires were fed into the test section housing through two Conax feed-throughs. A 0.16 cm (0.0625 in.) tube was placed vertically along the centerline of the bed to position the thermocouples. A data acquisition system having a voltage measuring capability of 0.5 V with a resolution of 12 bits, plus the sign bit, was calibrated and used to record the thermocouple data. The pressure in the test section was measured using a Heise absolute pressure gage, having a least division of 0.345 kPa (0.05 psia). Pressure fluctuations of 0.69 kPa (0.1 lbf in.$^{-2}$) were observed during experimental runs. The steam leaving the test section was condensed, and the average flow rate determined by directly measuring the collection rate over a specified time period.

The weight of the alumina particles was independently determined using a Mettler P-22 balance, having a least division of 0.1 g. The particles were weighed at room conditions, after oven drying, and after soaking in distilled water for various periods of time. The particles were soaked in distilled water for 24 h prior to each experimental run; additional time did not result in any further change in weight of the particles. The drying experiment was concluded when the load cell readings showed no further change in weight. After each experimental run the test section was dismantled, and the dried particles re-weighed on the balance to confirm the load cell results. Agreement between the load cell output and the values measured by the balance was excellent, within 1% for all runs. Also, the particles were placed in an oven at 150°C to determine the remaining moisture after steam drying. Additional weight loss after steam drying was never greater than 0.5% of the dry weight of the particles, which corresponds to a maximum of 1.5% of the initial moisture content.

## MODEL

The goal of the present model is to describe the drying process in a packed bed where the working fluid or drying medium is superheated steam. The drying process in a packed bed may begin with the packing temperature below the saturation temperature of the steam. As such, condensation may occur in the bed during start-up. Condensation is modeled in the present study at any point where heat transfer occurs from the steam to the particles after the steam has cooled to the saturation temperature. When drying with superheated steam, the local rate of vapor transport at the particle surface is not limited by mass transfer resistance, as would be the case in air drying, and thus the rate of evaporation from the surface is heat transfer limited. The current model employs volume averaged equations for the porous medium formed by the discrete particles. The heat transfer from the steam to the particles is described by a convective boundary condition at the particle to fluid interface; thus the driving potential for this heat transfer is the temperature difference between the particle surface and the steam.

Traditionally, the effect of intraparticle temperature gradients (particle Biot number effects) have been modeled through modifications to the heat transfer coefficient [25]. In the present model, this approach was deemed insufficient and an alternative procedure proposed. For the present study, the surface temperature of a single particle is predicted and incorporated into the volume averaged equations governing the fluid temperature in the packed bed. The single particle model will first be described, and subsequently the model for the packed bed, which incorporates the results of the single particle model.

*Single particle model*

The drying of a single spherical porous particle which is initially saturated with a liquid is modeled. The model proposed here *assumes* that heat transfer is the controlling mechanism for drying, that drying occurs from a receding interface between a wet and dry region within the particle, and that no liquid is transported to the surface of the particle during the drying process. Recent studies indicate that thin film evaporation within the pores of a material being dried may play an important role in the constant drying rate period [26, 27], and that liquid transport may not be the dominant factor during constant rate drying. The present model assumes a spherical porous particle having a known initial temperature distribution and moisture content, and subject to a uniform convective environment of superheated vapor of the same liquid as contained in the particle. For simplicity, the liquid and vapor will be discussed as if they were water, but the analysis is not restricted to any particular liquid. The particle is assumed to have a void fraction, $\phi$, defined as the ratio of the volume within the particle occupied by water (liquid+vapor) to the total volume. Drying begins when the surface temperature of the particle reaches the saturation temperature, for the present model assumed to be the saturation temperature for pure water, neglecting pressure changes within the particle and adsorption. The drying interface is assumed to be at this saturation temperature. Conduction occurs from the particle surface to the drying interface, and from the drying interface to the interior of the particle. After the drying interface has moved into the particle, the particle would exist in the condition shown in Fig. 3. Region I contains liquid water in the porous solid; the water is evap-

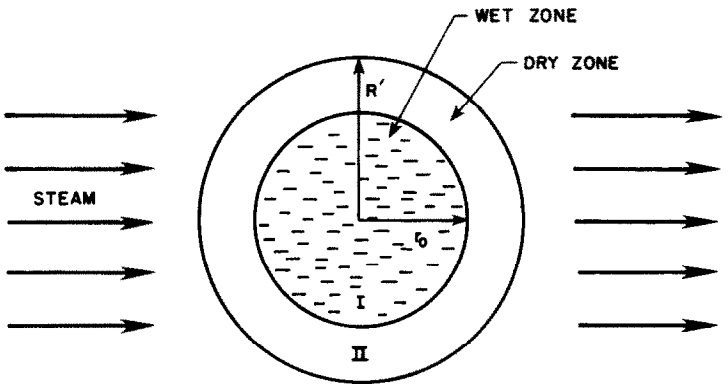


FIG. 3. Identification of drying regions for a spherical particle.

orating at the interface between Regions I and II. Capillary forces within the pores are assumed negligible, so that no liquid is transported to the surface of the particle by this mechanism. Evaporation from the drying interface is a result of heat transfer from the surface of the particle to the interface. This heat transfer occurs by conduction through the porous material which comprises the particle.

The following non-dimensional variables are defined for the spherical geometry

$$r = \frac{r'}{R'}$$

$$t = \frac{k_0}{\rho_0 c_0}\frac{t'}{(R')^2}$$

$$T = \frac{T' - T'_{sat}}{T'_{in} - T'_{sat}} \tag{1}$$

as the non-dimensional distance, time, and temperature, respectively. The governing equations may then be written

$$\frac{\partial^2 T}{\partial r^2} + \frac{2}{r}\frac{\partial T}{\partial r} = \beta_1 \frac{\partial T}{\partial t},\quad t > 0;\ 0 \leqslant r \leqslant r_0(t)$$

$$\frac{\partial^2 T}{\partial r^2} + \frac{2}{r}\frac{\partial T}{\partial r} = \beta_2 \frac{\partial T}{\partial t},\quad t > 0;\ r_0(t) \leqslant r \leqslant 1.0 \tag{2}$$

where

$$\beta_1 = \frac{k_0}{k_1}\frac{\rho_1 c_1}{\rho_0 c_0},\quad \beta_2 = \frac{k_0}{k_2}\frac{\rho_2 c_2}{\rho_0 c_0}.$$

The boundary condition at $r = 1$ is

$$\frac{\partial T}{\partial r} = -Bi_1\, T - Bi_1\, T_\infty,\quad r_0(t) = 1.0$$

$$\frac{\partial T}{\partial r} = -Bi_2\, T - Bi_2\, T_\infty,\quad r_0(t) < 1.0 \tag{3}$$

where

$$T_\infty = \frac{T'_{sat} - T'_\infty}{T'_{in} - T'_{sat}}$$

and at $r = 0$

$$\frac{\partial T}{\partial r} = 0 \tag{4}$$

with the initial condition $T = 1$ at $t = 0$. At the interface

$$\frac{dr_0}{dt} = -\lambda_1\left[\frac{\partial T}{\partial r}\right]^{I} + \lambda_2\left[\frac{\partial T}{\partial r}\right]^{II} \tag{5}$$

where

$$\lambda_1 = \frac{k_1}{k_0}\left[\frac{c_0\rho_0}{\rho_\ell \phi h_{fg}}\right](T'_{in} - T'_{sat})$$

$$\lambda_2 = \frac{k_2}{k_0}\left[\frac{c_0\rho_0}{\rho_\ell \phi h_{fg}}\right](T'_{in} - T'_{sat}). \tag{6}$$

The temperature boundary condition at the interface is $T = 0$ at $r = r_0(t)$. Equations (1)–(6) comprise the governing equations and boundary conditions, in non-dimensional variables, which describe the temperature distribution and location of the drying interface for a spherical particle.

Solution of the model proposed above is accomplished using finite differences. Several numerical schemes relating to moving boundary problems have been proposed, which differ primarily in the way they treat both the moving interface and the establishment of a grid. The numerical solutions to these problems are easier to implement for fixed temperature external boundary conditions; convective boundary conditions, as in the present case, may give rise to numerical instabilities as noted by Shamsundar [28]. Numerical methods for a one-dimensional moving boundary problem have been classified by Crank and Gupta [29] as fixed grid methods or variable grid methods. Variable grid methods are those where either the grid size or the time step is varied such that the

moving interface is located on a grid line at each successive time step. Douglas and Gallie [30] and Gupta and Kumar [31] examined methods using variable time steps. Murray and Landis [32] kept the number of spatial intervals between the boundary and the moving interface constant, and since the number of nodes is constant, the grid spacing changes with time. Crank and Gupta [29] avoided the complications due to unequal grid size near the moving boundary by moving the entire uniform grid system with the velocity of the moving boundary.

In fixed grid methods, the phase-change interface will usually be located between two neighboring grid points. Crank [33] used interpolation of the Lagrangian type on three points near the interface, and developed an explicit solution method. Lazaridis [34] used explicit finite-difference approximations on a fixed grid to solve two-phase solidification problems in both two and three dimensions.

For the present solution, the sphere is divided into $N$ equally spaced divisions with spacing $\Delta r$. The Crank–Nicholson method is used to expand equation (2) in finite-difference form as

$$\frac{i-2}{i-1}T_{i-1}^{j+1}-\left[2+\frac{2\beta_1(\Delta r)^2}{(\Delta t)}\right]T_i^{j+1}+\frac{i}{i-1}T_{i+1}^{j+1}$$
$$=-\frac{i-2}{i-1}T_{i-1}^{j}+\left[2-\frac{2\beta_1(\Delta r)^2}{(\Delta t)}\right]T_i^{j}-\frac{i}{i-1}T_{i+1}^{j}$$
$$\text{when } (i\Delta r)<r_0(t) \quad (7)$$

and

$$\frac{i-2}{i-1}T_{i-1}^{j+1}-\left[2+\frac{2\beta_2(\Delta r)^2}{(\Delta t)}\right]T_i^{j+1}+\frac{i}{i-1}T_{i+1}^{j+1}$$
$$=-\frac{i-2}{i-1}T_{i-1}^{j}+\left[2-\frac{2\beta_2(\Delta r)^2}{(\Delta t)}\right]T_i^{j}-\frac{i}{i-1}T_{i+1}^{j}$$
$$\text{when } (i\Delta r)>r_0(t).$$

These equations are not valid for the nodal points adjacent to the moving interface. The location of the evaporation front is determined at each time step by evaluating the interface condition. Different finite-difference formulations are necessary at the moving interface, and for the case where the interface crosses a nodal location during a time step. Further details of the model development may be found in ref. [35].

The finite-difference form of the equation for the location of the moving boundary is developed by using the Lagrangian interpolation formulas [36] for the derivative of temperature. When a three point interpolation formula is used, the interface is determined by

$$\frac{dr_0}{dt}=\lambda_2\Delta_2^{j+1}-\lambda_1\Delta_1^{j+1} \quad (8)$$

where

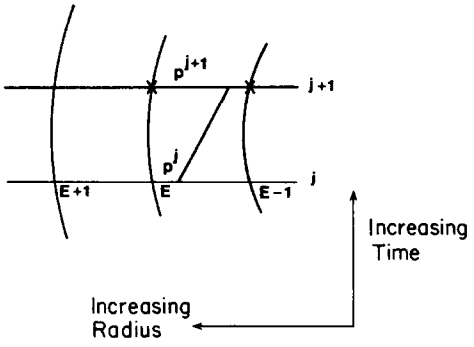


FIG. 4. Computational grid and time domain.

$$\Delta_1=\frac{1}{(\Delta r)}\left[\frac{1-P^{j+1}}{2-P^{j+1}}T_{E-2}^{j+1}-\frac{2-P^{j+1}}{1-P^{j+1}}T_{E-1}^{j+1}\right]$$
$$\Delta_2=\frac{1}{(\Delta r)}\left[-\frac{P^{j+1}}{P^{j+1}+1}T_{E-1}^{j+1}+\frac{1+P^{j+1}}{P^{j+1}}T_E^{j+1}\right]. \quad (9)$$

The computational grid and time domain are shown in Fig. 4. When $P^{j+1}$ is very small or is very close to 1, the interpolation formulas become unstable. Under this condition, the interface node is eliminated from the interpolation scheme for the temperature.

*Packed bed model*

For the packed bed, it was assumed that the average flow was one-dimensional, and that the temperature distribution in the fluid phase could be described by a volume averaged form of the energy equation [37]

$$\varepsilon\rho c\frac{\partial\chi}{\partial t}+\varepsilon\rho cu\frac{\partial\chi}{\partial x}=\varepsilon k_e^x\frac{\partial^2\chi}{\partial x^2}+ha(T_s'-\chi). \quad (10)$$

When drying a particle with superheated vapor, there is no mass transfer resistance, and thus the rate of evaporation is determined solely by the rate of heat transfer to the drying interface [18]. The equation describing the steam temperature distribution is approximated by a fully implicit finite-difference equation. The preservation of the transportive property for the convective term through upwind differencing is necessary for the convergence of the implicit formulation. The resulting finite-difference equation for the steam temperature is, for the general node

$$-(A+B)\chi_{i-1}^{j+1}+(1+A+2B+C)\chi_i^{j+1}$$
$$-B\chi_{i+1}^{j+1}=\chi_i^{j}+C(T_{si}')^{j+1} \quad (11)$$

where

$$A=\frac{u(\Delta t)}{(\Delta x)},\quad B=\frac{k_e^x(\Delta t)}{\rho c(\Delta x)^2},\quad C=\frac{ha(\Delta t)}{\rho c\varepsilon}. \quad (12)$$

With the surface temperature of the solid as input from the single particle model, the resulting tri-

diagonal coefficient matrix can be solved directly using the Thomas algorithm [38].

The transient solution begins with an initial temperature distribution in the solid and fluid phases within the bed, and a specified inlet condition for the steam flow. The solution follows a predictor–corrector algorithm for which the first step in the solution procedure is determining the steam temperature at the future time step, including checking for condensation. The single particle model is then solved at each grid point in the packed bed, and the drying conditions of the single particle determined. The steam temperature can then be updated based on the calculated particle surface temperatures. These steps are repeated at one location in time until convergence in the surface temperature is achieved. The solution procedure may then step forward in time, to once again be repeated to convergence.

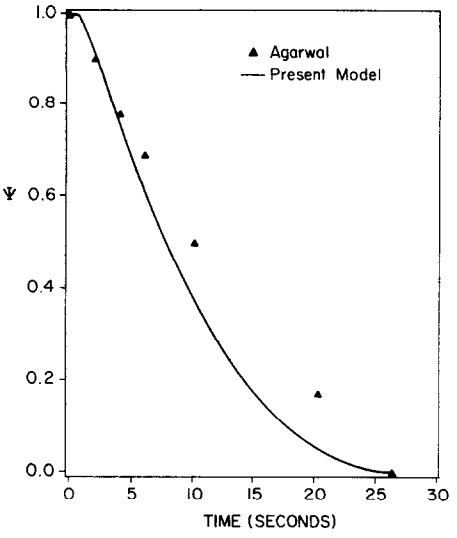


FIG. 5. Comparison of drying predictions from the present model and that of Agarwal *et al.* [23].

## RESULTS

The present study involved experimental measurements of overall drying rates and temperature distribution in a packed bed, and computational predictions of both evaporation from a single particle, and the overall drying rate in a packed bed. Drying experiments were performed for a range of Reynolds numbers, achieved by changes in the steam flow rate, the particle size and the inlet steam conditions.

Some basic assumptions are implicit in the analysis of the experimental data and presentation of the experimental results:

(1) The steam inlet temperature and flow rate are constant. As measured, the steam temperature at the bed inlet and the mass flow rate did not change by more than 0.3 and 3%, respectively, from the set point values.

(2) Energy losses from the walls of the test section were negligible, resulting in no radial heat transfer. The temperature variations were less than 2% of the total temperature rise above the initial conditions in the bed.

(3) Axial conduction in the bed was negligible (neglected for analysis of the experimental data, but included in the model for generality); the Peclet number was determined to be sufficiently high that axial convective transport dominated for the flow rates tested. Values of the Peclet number ranged from 1245 to 2215 in this study.

(4) The fluid-to-particle heat transfer coefficient was the same for all phases of drying.

(5) The effect of fluid momentum or pressure drop on the measured bed weight was determined to be negligible; in addition, the mass evolution did not appreciably increase the flow rate as the steam passed through the bed.

*Results from the single particle model*

The numerical model for evaporation from a single particle into superheated vapor was compared to existing solutions and the convergence of the routine demonstrated through computational experiment. In the limiting case when the volume fraction of liquid in a single particle is 1, the problem reduces to a classical Stefan problem. Comparisons with the solutions of Tao [39] were made, and the predictions of the present model, with the volume fraction of liquid equal to 1, were identical to those of Tao.

Agarwal *et al.* [23] modeled the drying problem in a spherical geometry using a pseudo-steady approximation for the surface temperature, and assuming no heat transfer to the wet core. A comparison between the present model and Agarwal *et al.*'s results is presented in Fig. 5. Input values are listed in Table 1. As expected, heat transfer to the core region (Region I) reduces the drying rate in the early stages of drying below that predicted by Agarwal *et al.* [23]. In contrast to previous models, the present model predicts the temperature distribution within the particle during drying, in both the wet and dry regions.

Figure 6 shows the temperature distributions at the point in time when evaporation first begins in the particle, or when the surface temperature first reaches saturation. The particle begins from a uniform initial temperature. For increasing Biot number, the tem-

Table 1. Input property values for comparison with Agarwal *et al.* [23]

| Solid | Liquid |
|---|---|
| $\alpha = 0.1\ \text{mm}^2\ \text{s}^{-1}$ | $c = 1.0\ \text{cal g}^{-1}\ \text{C}^{-1}$ |
| $c = 0.35\ \text{cal g}^{-1}\ \text{C}^{-1}$ | $h_{lg} = 570\ \text{cal g}^{-1}$ |
| $\rho = 1.15\ \text{g cm}^{-3}$ | $\rho = 1\ \text{g cm}^{-3}$ |
| $d_p = 4\ \text{mm}$ | $k = 0.614\ \text{W m}^{-1}\ \text{C}^{-1}$ |
| $Bi_d = 4$ | $T_s = 800\ \text{K}$ |
| $\phi = 0.375$ | |

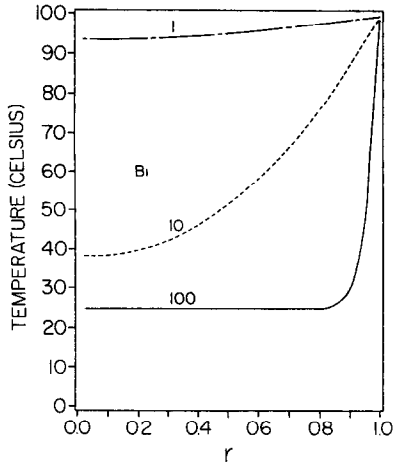


FIG. 6. Temperature distribution corresponding to the start of drying for three Biot numbers.

perature differences within the particle are larger. Figure 7 shows the temperature distributions for three Biot numbers after the location of the interface between the wet and dry regions has moved 25% of the radius into the particle. Even after this much drying has occurred, the wet core region of the particle may not be uniform at the saturation temperature.

*Packed bed model*

The single particle model was incorporated into a general model for packed bed drying. To demonstrate the validity of the model predictions, the computational routine was examined for both spatial and temporal convergence, and an energy balance was performed at each time step. Results from this model with the volume fraction of liquid within the particle set to zero were also compared with the experimental results of Vanden Broek and Clark [40]. They measured temperature distributions in a packed bed subject to a step change in inlet fluid temperature. Comparisons between measured and computed values were consistent with those of previous models [41]. These studies demonstrated that the computational routine was consistent with the proposed finite-difference equations, and that the predictions represented accurately a converged solution to the governing equations.

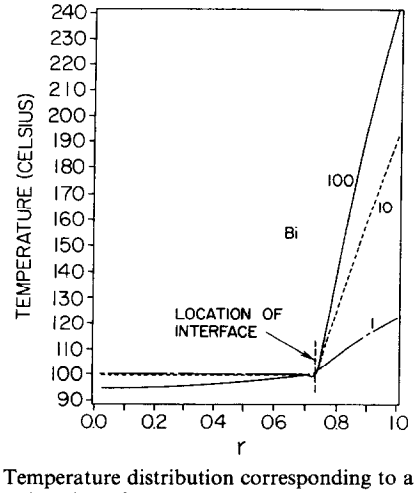


FIG. 7. Temperature distribution corresponding to a drying interface location of $r_0'/R' = 0.25$, for three Biot numbers.

The time step for the routine was chosen such that the moving interface within the particle did not cross two spatial grid locations during one time step. An optimum time step for each particle size was determined by performing computational experiments with the single particle model. For example, for the particle size of 1.1 cm diameter, it was determined that a time step of 1 s and 32 spatial grid locations were appropriate, as there was no appreciable difference in the result if the time step was reduced or the number of spatial grid locations increased. The single particle time step was more limiting than the time step required for convergence of the overall packed bed model. The consistency of the numerical model was demonstrated further by performing an energy balance for a control volume containing the packing. The total enthalpy change for the fluid at the inlet and exit of the bed was compared to the energy change for the particles within the control volume. For all computational results, after the first few time steps the difference in these two values was already less than 1% (at very small times the two energy terms are extremely small, which causes an error in their difference of approximately 5%).

*Drying results*

An overall heat transfer coefficient was calculated by solution of an integral form of the energy equation for the packed bed. This equation was applied to the entire bed in the falling rate period of drying. The temperatures at all locations within the bed during the falling rate period were above saturation temperature of the steam, allowing the determination of the heat transfer coefficient. From the measured temperature profile within the bed, and using the total surface area of the particles as the heat transfer area, an overall heat transfer coefficient could be calculated.

The application of the First Law required measured values of the transient moisture content in the bed, drying rate, transient temperature profile in the bed, and the steam flow rate and inlet and exit conditions. Fourteen individual runs were performed; Table 2 provides the experimental conditions for each run. A complete uncertainty analysis of the effects of steam flow rate measurement inaccuracies, the effect of the momentum of the steam on the load cell output, and the uncertainty in the load cell measurements was performed [42]. For the analysis of the experimental data it is assumed that there is no axial conduction, and that the lateral boundaries are insulated. For the purpose of determining the overall heat transfer coefficient, the energy equation was solved in finite-difference form, resulting in the heat transfer

Table 2. Experimental conditions

| Run No. | Inlet temperature (°C) | Bed pressure (kPa) | Bed length (cm) | Particle diameter (cm) | Steam flow rate (kg h$^{-1}$) | Reynolds number |
|---|---|---|---|---|---|---|
| 1 | 176.7 | 144.7 | 17.8 | 1.11 | 86.2 | 483 |
| 2 | 176.7 | 144.7 | 17.8 | 1.11 | 111.2 | 623 |
| 3 | 176.7 | 144.7 | 17.8 | 1.11 | 121.6 | 682 |
| 4 | 176.7 | 144.7 | 17.8 | 1.11 | 139.3 | 781 |
| 5 | 176.7 | 144.7 | 17.8 | 0.56 | 90.7 | 254 |
| 6 | 176.7 | 144.7 | 17.8 | 0.72 | 93.0 | 335 |
| 7 | 176.7 | 144.7 | 17.8 | 0.87 | 88.5 | 389 |
| 8 | 154.4 | 144.7 | 17.8 | 0.87 | 95.3 | 436 |
| 9 | 187.8 | 144.7 | 17.8 | 0.87 | 93.9 | 397 |
| 10 | 204.4 | 144.7 | 17.8 | 0.87 | 88.9 | 363 |
| 11 | 176.7 | 144.7 | 17.8 | 0.72 | 132.5 | 478 |
| 12 | 176.7 | 144.7 | 10.2 | 0.72 | 135.7 | 489 |
| 13 | 176.7 | 179.2 | 17.8 | 0.55 | 138.4 | 388 |
| 14 | 176.7 | 144.7 | 17.8 | 0.55 | 88.5 | 248 |

coefficient. A detailed description of the calculation of the heat transfer coefficient is given in ref. [43]. The results of these calculations are presented in dimensionless form in Fig. 8. For both the Reynolds number and Nusselt number, the characteristic length was the particle diameter. Property values of the fluid are evaluated at the inlet temperature. The curve shown in Fig. 8 is a linear least squares fit to the experimental data, and may be expressed as

$$Nu = 1.8Re^{0.585}. \quad (13)$$

Dimensional analysis indicates that the Prandtl number should be included in such a correlation; based on numerous previous studies of heat transfer in packed beds, the correlating equation derived from the present experimental data may be extended to other fluids by including a Prandtl number effect

$$Nu = 1.8Re^{0.585}\,Pr^{1/3}. \quad (14)$$

Uncertainty bounds for the Nusselt and Reynolds numbers are shown for four points in Fig. 8.

Model predictions were compared with measured evaporation rates and temperature profiles. Figures 9 and 10 compare measured and predicted values of the moisture content in the bed as a function of time for Reynolds numbers of 781 and 254, for two particle sizes. The predictions compare favorably with the measured values. The prediction for condensation is consistent with the measured trends, but precise evaluation of these predictions is hindered by the fact that the experimental uncertainty in the weight of the bed is larger at the beginning of the experiment. All 14 experimental runs were compared with model predictions, and agreement similar to that presented in Figs. 9 and 10 was found. Table 3 shows the initial condensation, drying rates in the constant rate period, and the total drying time for each run, along with the experimental conditions.

The process of drying in a packed bed of significant depth has not been examined in detail previously for

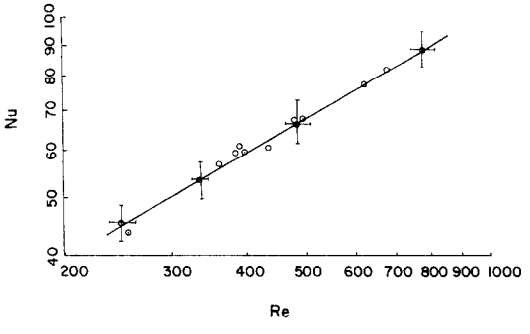


FIG. 8. Nusselt number variation with Reynolds number for drying in the present experiment.

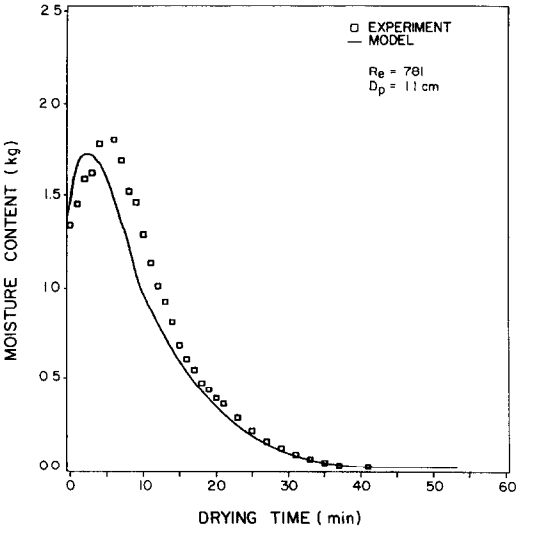


FIG. 9. Comparison of model predictions with measured values of instantaneous moisture content for steam flow of 139.3 kg h$^{-1}$.

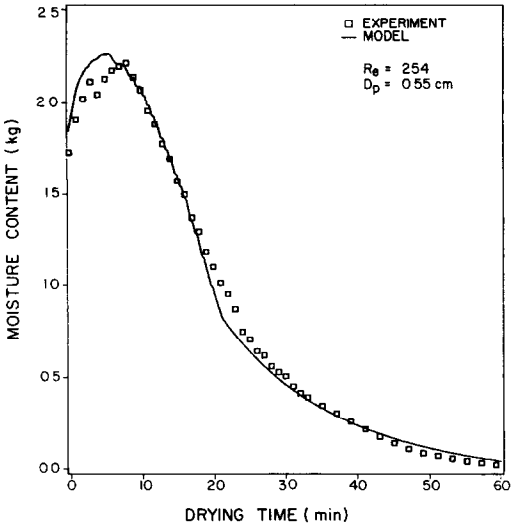


FIG. 10. Comparison of mode predictions with measured values of instantaneous moisture content for steam flow of 90.7 kg $h^{-1}$.

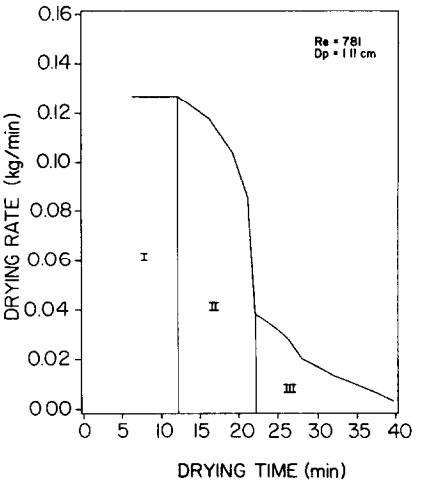


FIG. 11. Experimentally determined drying rate curve for a Reynolds number of 781 and a particle diameter of 1.11 cm.

the case of superheated steam drying. The process of drying in a packed bed is observed to occur in three phases, as shown in Figs. 11 and 12. Consider the case of a packed bed which has reached the saturation temperature of the steam throughout. After this start-up period, there is a period of time for which the drying rate is constant, labeled Phase I in Fig. 11. During this period, the steam temperature decreases from the inlet temperature to the saturation temperature over some length along the flow direction. This temperature change over a short distance along the flow direction is called a thermocline. During Phase I, the surface temperature of all the particles in the bed is the saturation temperature of the steam, resulting in the constant drying rate.

Phase II of the drying rate curve exhibits a continuously decreasing rate of overall drying. This results physically from particles in the upper regions

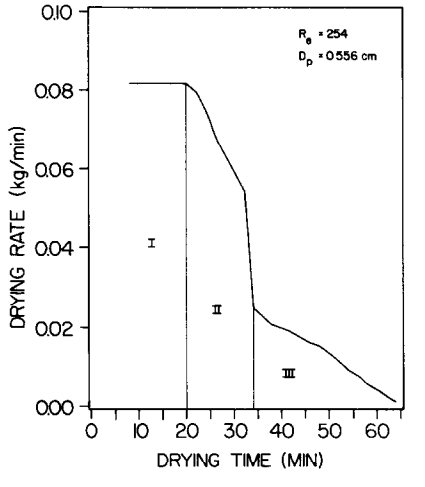


FIG. 12. Experimentally determined drying rate curve for a Reynolds number of 254 and a particle diameter of 0.556 cm.

Table 3. Drying results

| Run No. | Initial moisture (kg) | Condensation (% initial moisture) | Maximum drying rate (kg $min^{-1}$) | Drying time (min) |
|---|---|---|---|---|
| 1 | 1.34 | 36 | 0.077 | 51 |
| 2 | 1.37 | 36 | 0.100 | 59 |
| 3 | 1.36 | 36 | 0.109 | 45 |
| 4 | 1.34 | 39 | 0.127 | 41 |
| 5 | 1.72 | 28 | 0.082 | 65 |
| 6 | 1.72 | 21 | 0.082 | 63 |
| 7 | 1.75 | 12 | 0.082 | 58 |
| 8 | 1.63 | 20 | 0.059 | 52 |
| 9 | 1.74 | 14 | 0.100 | 53 |
| 10 | 1.75 | 12 | 0.113 | 52 |
| 11 | 1.69 | 23 | 0.118 | 43 |
| 12 | 0.91 | 27 | 0.122 | 30 |
| 13 | 1.81 | 20 | 0.122 | 47 |
| 14 | 1.81 | 20 | 0.082 | 62 |

of the bed entering the falling rate period of drying. The temperature of these particles rises above the saturation temperature of the steam, and thus a portion of the sensible energy of the steam no longer provides evaporation of liquid water, but rather goes to elevating the temperature of the particles in the upper regions of the bed.

A reasonably sharp transition to Phase III of drying occurs when the entire bed enters the falling rate period of drying. At this point, all of the particle surface temperatures are above saturation, the bed is largely dry, and the drying rate continually decreases to zero.

Figure 13 is a plot of the transient temperature distribution in the bed during drying, for a Reynolds number of 781, and corresponds to the drying rate curve shown in Fig. 11. Several observations can be made from the behavior of the temperature curves. The beginning of Phase II of the drying process is seen to occur after approximately 12 min. Also at approximately 12 min the temperature of the first thermocouple rises above the saturation temperature. This thermocouple is located at a depth of 2.5 cm (1 in.) into the packing. Clearly, the physical occurrence of the rise in particle temperature in the upper region of the bed signals the start of Phase II, where a portion of the bed experiences constant rate drying, and a portion is in the falling rate period. As previously described, Phase III of the drying process begins when all of the bed enters the falling rate period. Almost exact correspondence exists between the rise in the last thermocouple temperature and the beginning of Phase III drying as determined from the drying rate curve. This last thermocouple is located 2.5 cm (1 in.) from the exit of the bed. Comparisons between the model and measured values of the temperature distribution in the bed provide reasonable qualitative agreement. The times at which the temperature at various axial locations rises above the saturation temperature is correctly predicted throughout the bed. Predicted temperature distributions are in excellent agreement with the experimental findings until the falling rate period is reached locally. However, the present model fails to accurately predict the temperatures during the falling rate period. This failure to accurately predict the temperature distribution during Phase III corresponds to the removal of the final 10% of moisture from the particles. The observed differences in temperature distribution may result from the heat of adsorption effects during Phase III; in addition some aspects of the axial thermal dispersion may not be accurately described. Figure 9 demonstrates that the drying rate predictions are not adversely affected by the lack of agreement in the temperature distribution during Phase III. Further refinement of the model, perhaps through improvements to the heat transfer coefficient model and modeling of adsorption would not result in significantly improved predictions of the overall drying rate.

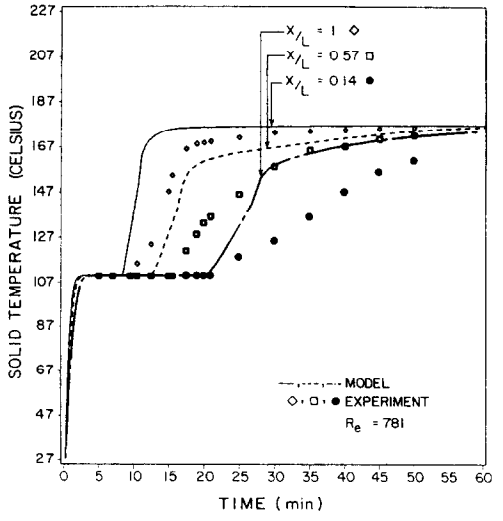


FIG. 13. Comparison of measured and predicted instantaneous bed temperatures for a steam flow rate of 139.3 kg $h^{-1}$.

## CONCLUSIONS

An experimental and computational study of drying in a packed bed of porous particles using steam as the drying medium has been conducted. The experimental results indicate that drying in a packed bed of significant depth occurs in three phases, which are a result of the nature of the drying process for the individual particles. The three phases of drying correspond to situations where the entire bed is in the constant rate drying period, a portion of the bed is in the falling rate period, and when the entire bed is in the falling rate period.

A thermally controlled model of drying in superheated steam has been proposed for a single spherical porous particle, and incorporated into an overall model of drying in a packed bed. Model results agree favorably with measured drying curves over a range of Reynolds numbers and particle sizes. The model provides the capability to predict condensation during the initial heating of the packed bed, before drying begins. The model provides reliable predictions of superheated steam drying in a packed bed.

Values of the heat transfer coefficient were calculated through application of an integral form of the First Law of Thermodynamics during the falling rate period of drying (Phase III). A correlating equation was derived for heat transfer for superheated steam drying in a packed bed.

*Acknowledgements*—The authors wish to acknowledge the support of the South Carolina Energy Research and Development Center and the Department of Mechanical Engineering for this research.

## REFERENCES

1. O. E. Potter, Approaches to more economical drying of particles and lumps. In *Drying 1980* (Edited by A. S. Mujumdar), p. 396. Hemisphere, New York (1980).

2. W. K. Lewis, The rate of drying of solid materials, *Ind. Engng Chem* **13,** 427 (1921).
3. T. K. Sherwood, Application of the theoretical diffusion equations to the drying of solids, *Trans. Am. Inst. Chem. Engng* **27,** 190 (1931).
4. E. R. Gilliland and T. K. Sherwood, The drying of solids VI: diffusion equations for the period of the constant drying rate, *Ind. Engng Chem.* **25**(11), 34–36 (1933).
5. L. A. Richards, Capillary conduction of liquids through porous medium, *J. Appl. Phys.* **1,** 318 (1931).
6. D. A. Hougen, H. J. McCauley and W. R. Marshall, Jr., Limitations of diffusion equations in drying, *Trans. Am. Inst. Chem. Engng* **36,** 183 (1940).
7. O. Krischer, The heat, moisture and vapor movement during drying porous material, *VDI Z.* **1,** 17–24 (1940).
8. J. R. Phillip and D. A. De Vries, Moisture movement in porous material under temperature gradient, *Trans. Am. Geophys. Un.* **38,** 222–232 (1957).
9. D. Berger and D. C. T. Pei, Drying of hygroscopic capillary solids—a theoretical approach, *Int. J. Heat Mass Transfer* **16,** 293 (1973).
10. A. V. Luikov, Systems of differential equations of heat and mass transfer in capillary porous bodies, *Int. J. Heat Mass Transfer* **18,** 1–14 (1975).
11. M. A. Stanish, G. S. Schajer and F. Kayiham, A mathematical model of drying for hygroscopic porous media, *A.I.Ch.E. Jl* **32,** 1301 (1986).
12. K. Min and H. W. Emmons, The drying of porous media, *Proc. 1972 Heat Transfer and Fluid Mech. Inst.* Stanford University Press, Stanford, California (1972).
13. A. Dayan and E. L. Gluekler, Heat and mass transfer within an intensely heated concrete slab, *Int. J. Heat Mass Transfer* **25,** 1461–1467 (1982).
14. E. Hausbrand, *Drying by Means of Air and Steam* (3rd Edn). Scott, Greenwood and Son, London (1924).
15. L. Wenzel and R. R. White, Drying of granular solids in superheated steam, *Ind. Engng Chem.* **43,** 1829 (1951).
16. T. Yoshida and T. Hyodo, Evaporation of water in air, humid air, and superheated steam, *Ind. Engng Chem.* **9**(2), 207–214 (1970).
17. M. Hasan, A. S. Mujumdar and M. Al-Taleb, Evaporation from flat surfaces into unsaturated and superheated solvent vapor. In *Drying 86*, Vol. 2, pp. 604–616. Hemisphere, New York (1986).
18. E. Loo and A. S. Mujumdar, A simulation model for combined impingement and through drying using superheated steam as the drying medium. In *Drying 84* (Edited by A. S. Mujumdar). Hemisphere, New York (1984).
19. J. Meunier and R. J. Munz, Flash drying with superheated steam—a mathematical model. In *Drying '86* (Edited by A. S. Mujumdar). Hemisphere, New York (1986).
20. J. G. Salin, Steam drying of wood particles for particle board. In *Drying '86* (Edited by A. S. Mujumdar). Hemisphere, New York (1986).
21. K. Kato, S. Ohmura, D. Taneda, I. Onozawa, K. Shimura and A. Iijima, Drying characteristics in a packed fluidized bed dryer, *J. Chem. Engng Japan* **14,** 365–371 (1981).
22. M. Hasatani and N. Arai, Unsteady, 2-D heat and mass transfer in a packed bed of fine particles with an endothermic process, *Chem. Engng Commun.* **10,** 223–242 (1981).
23. P. K. Agarwal, W. E. Genetti and Y. Y. Lee, Coupled drying and devolatization of wet coal in fluidized beds, *Chem. Engng Sci.* **41,** 2373 (1986).
24. H. W. Cheong, G. V. Jeffreys and C. J. Mumford, A receding interface model for the drying of slurry droplets, *A.I.Ch.E. Jl* **32,** 1334 (1986).
25. A. V. Bradshaw, A. Johnson, N. H. MaLachlan and Y.-T. Chiu, Heat transfer between air and nitrogen and packed beds of non-reacting solids, *Trans. Instn Chem. Engng* **48,** T77 (1970).
26. S. L. Cheng, Jer Ru Maa and Yu Min Yang, Interfacial phenomena of capillary evaporation, *Proc. Sixth Int. Drying Symp.*, Versailles, France, p. 479 (1988).
27. E. U. Schlunder, On the mechanism of the constant rate drying period, *Proc. Sixth Int. Drying Symp.*, Versailles, France, p. 487 (1988).
28. N. Shamsundar, Comparison of numerical methods for diffusion problems with moving boundaries. In *Moving Boundary Problems* (Edited by D. G. Wilson, A. D. Solomon and P. T. Boggs), p. 165. Academic Press, New York (1978).
29. J. Crank and R. S. Gupta, A method for solving moving boundary problems in heat flow using cubic splines or polynomials, *J. Inst. Math. Applic.* **10,** 296 (1972).
30. J. Douglas and T. M. Gallie, On the numerical integration of a parabolic differential equation subject to a moving boundary condition, *Duke Math. J.* **22,** 557 (1955).
31. R. S. Gupta and D. Kumar, Variable time step methods for one-dimensional Stefan problem with mixed boundary condition, *Int. J. Heat Mass Transfer* **24,** 251 (1981).
32. W. D. Murray and F. Landis, Numerical and machine solutions of transient heat conduction problems involving melting or freezing, *J. Heat Transfer* **81,** 106 (1959).
33. J. Crank, Two methods for the numerical solution of moving-boundary problems in diffusion and heat flow, *Q. J. Mech. Appl. Math.* **10,** 220 (1957).
34. A. Lazaridis, A numerical solution of the multidimensional solidification (or melting) problem, *Int. J. Heat Mass Transfer* **13,** 1459 (1970).
35. J. A. Khan and D. E. Beasley, A model for thermally controlled drying of a porous sphere using superheated vapor. In *Collected Papers in Heat Transfer—1988* (Edited by K. T. Yang), ASME-HTD-Vol. 104 (1988).
36. J. Crank, *Free and Moving Boundary problems*. Clarendon Press, Oxford (1984).
37. S. Whitaker, Simultaneous heat, mass and momentum transfer in porous media: a theory of drying, *Adv. Heat Transfer* **13,** 119 (1977).
38. D. A. Anderson, J. C. Tannehill and R. H. Pletcher, *Computational Fluid Mechanics and Heat Transfer*. Hemisphere, Washington, DC (1984).
39. L. C. Tao, Generalized numerical solutions of freezing a saturated liquid in cylinders and spheres, *A.I.Ch.E. Jl* **13,** 165 (1967).
40. C. D. Vanden Broek and J. A. Clark, Heat transfer in a column packed with spheres. In *Heat Exchange and Solar Energy*, Von Karman Institute for Fluid Dynamics Lecture Series. Brussels, Belgium (1980–82).
41. D. E. Beasley and J. A. Clark, Transient response of a packed bed for thermal energy storage, *Int. J. Heat Mass Transfer* **27,** 1659 (1984).
42. J. A. Khan, Evaporation from a packed bed of porous particles into superheated vapor, Ph.D. Dissertation, Clemson University (1988).
43. B. Alatas, Superheated steam drying of spherical particles in packed beds, M.S. Thesis, Clemson University (1988).

## EVAPORATION A PARTIR D'UN LIT FIXE DE PARTICULES POREUSES DANS LA VAPEUR SURCHAUFFEE

**Résumé**—On conduit une étude expérimentale et numérique de l'évaporation dans la vapeur, à partir de particules poreuses disposées en lit fixe. Le but de cette étude est de développer un modèle prédictif du mécanisme de séchage dans des lits fixes avec la vapeur comme asséchant. La mesure directe du poids des particules d'alumine de diamètres différents dans un lit fixe conduit à une courbe continue de séchage. On considère plusieurs conditions opératoires et on développe une équation pour le coefficient global de transfert thermique. L'évaporation à partir d'une particule sphérique unique est modélisée en supposant qu'elle est pilotée thermiquement. Ce modèle est incorporé dans un autre concernant un lit fixe, pour prédire les flux de séchage globaux et locaux, aussi bien que les distributions de température dans le lit. Les résultats de cette étude indiquent que le séchage du lit de hauteur significative se fait en trois phases qui correspondent à des périodes où le lit entier est à vitesse de séchage constante, puis où il y a partiellement le régime de réduction et enfin quand tout le lit entier est dans le régime de réduction. L'existence de ces phases est confirmée par les distributions mesurées de température et les taux de séchage mesurés. Les prédictions de séchage global données par le modèle montrent un accord satisfaisant avec les courbes expérimentales de séchage.

## TROCKNUNG EINER SCHÜTTUNG AUS PORÖSEN PARTIKELN DURCH ÜBERHITZTEN DAMPF

**Zusammenfassung**—Die Verdampfung aus einer Schüttung, gebildet aus porösen Partikeln, im überhitzten Dampf wird experimentell und numersich untersucht. Das Ziel der Untersuchung ist die Entwicklung eines Modells zur Berechnung des Trocknungsvorgangs mit Dampf als Trocknungsmedium. Im Versuch wird der Gewichtsverlust von Partikeln aus Aluminiumoxid unterschiedlichen Durchmessers direkt gemessen, woraus sich eine vollständige kontinuierliche Trocknungskurve ergibt. Die Versuchsbedingungen werden über einen weiten Bereich variiert, es ergibt sich eine Korrelationsgleichung für den gemittelten Wärmeübergangskoeffizienten. Die Verdampfung in einer einzelnen porösen Kugel wird durch das Modell einer sich zurückziehenden Flüssigkeits-/Dampf-Grenzfläche im Inneren des Partikels nachgebildet. Dabei wird angenommen, daß der Trocknungsvorgang durch die Temperatur gesteuert wird. Das Modell für eine einzelne Kugel wird in das Gesamtmodell einer Schüttung eingefügt. Örtliche und gemittelte Trocknungsgeschwindigkeiten werden berechnet, ebenso der zeitliche Temperaturverlauf in der Schüttung. Die Ergebnisse der Untersuchung zeigen, daß die Trocknung in einer Schüttung mit signifikanter Schichtdicke in drei Phasen abläuft. Die drei Trocknungsphasen entsprechen dabei drei Zeitabschnitten, in denen die Schüttung entweder eine konstante Trocknungsgeschwindigkeit oder abnehmende Trocknungsgeschwindigkeiten aufweist—zunächst lokal, später an allen Stellen. Das Auftreten dieser drei Trocknungsphasen wird sowohl durch die gemessenen Temperaturverteilungen als auch die gemessenen Trocknungsverläufe bestätigt. Die berechneten mittleren Trocknungsgeschwindigkeiten zeigen eine günstige Übereinstimmung mit gemessenen Trocknungskurven.

## ИСПАРЕНИЕ ПЛОТНОГО СЛОЯ ЧАСТИЦ ПОРИСТОГО МАТЕРИАЛА В ПЕРЕГРЕТЫЙ ПАР

**Аннотация**—Экспериментально и численно исследуется процесс испарения частиц пористого материала, образующих слой, в перегретый пар. Целью работы является разработка расчетной модели сушки в плотных слоях с паром в качестве осушающей среды. В результате проведенных с помощью динамометрического датчика прямых экспериментальных измерений в процессе сушки веса частиц корунда различных диаметров в плотном слое получена нолная непрерывная кривая сушки. Оценивается диапазон условий эксперимента, и выводится обобщенное соотношение для коэффициента суммарного теплопереноса. Испарение единичной сферической частицы пористого материала моделируется как процесс, происходящий на заглубляющейся границе раздела жидкость/пар внутри частри частицы. Предполагается, что процесс сушки в единичной частице является термостатическим. При разработке общей модели сушки в плотном слое используется модель единичной частицы. Полученная модель позволяет рассчитать обую и локальную скорости сушки, а также нестационарное распределение температуры в упаковке. Результаты исследования показывают, что процесс сушки в плотном слое значительной глубины проходит три фазы. Эти фазы соответствуют периодам, когда сушка происходит с постоянной скоростью во всем слое, когда на некторых участках слоя сушка характеризуется падающей скоростью и когда она происходит с падающей скоростью во всем слое. Существование этих трех фаз процесса подтверждается измеренными распределениями температуры и скоростями сушки. Расчеты суммарной скорости сушки по предложенной модели удовлетворительно согласуются с измеренными кривыми сушки.